CHAPTER TWELVE

Conformationally Gated Electron Transfer in Nitrogenase. Isolation, Purification, and Characterization of Nitrogenase From *Gluconacetobacter diazotrophicus*

Cedric P. Owens[*,1], **Faik A. Tezcan**[†,1]

[*]Schmid College of Science and Technology, Chapman University, Orange, CA, United States
[†]University of California, San Diego, La Jolla, CA, United States
[1]Corresponding authors: e-mail address: cpowens@chapman.edu; tezcan@ucsd.edu

Contents

Methods in Enzymology, Volume 599
ISSN 0076-6879
https://doi.org/10.1016/bs.mie.2017.09.007

Abstract

Nitrogenase is a complex, bacterial enzyme that catalyzes the ATP-dependent reduction of dinitrogen (N_2) to ammonia (NH_3). In its most prevalent form, it consists of two proteins, the catalytic molybdenum-iron protein (MoFeP) and its specific reductase, the iron protein (FeP). A defining feature of nitrogenase is that electron and proton transfer processes linked to substrate reduction are synchronized by conformational changes driven by ATP-dependent FeP–MoFeP interactions. Yet, despite extensive crystallographic, spectroscopic, and biochemical information on nitrogenase, the structural basis of the ATP-dependent synchronization mechanism is not understood in detail. In this chapter, we summarize some of our efforts toward obtaining such an understanding.

Experimental investigations of the structure–function relationships in nitrogenase are challenged by the fact that it cannot be readily expressed heterologously in non-diazotrophic bacteria, and the purification protocols for nitrogenase are only known for a small number of diazotrophic organisms. Here, we present methods for purifying and characterizing nitrogenase from a new model organism, *Gluconacetobacter diazotrophicus*. We also describe procedures for observing redox-dependent conformational changes in *G. diazotrophicus* nitrogenase by X-ray crystallography and electron paramagnetic resonance spectroscopy, which have provided new insights into the redox-dependent conformational gating processes in nitrogenase.

Graphical Abstract

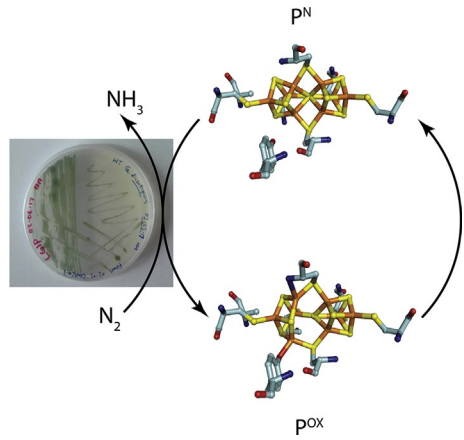

ABBREVIATIONS

ATP	adenosine triphosphate
Av	*Azotobacter vinelandii*
Cp	*Clostridium pasteurianum*
DG	docking geometry
DT	sodium dithionite

EPR	electron paramagnetic resonance
ET	electron transfer
FeP	iron protein
FPLC	fast protein liquid chromatography
Gd	*Gluconacetobacter diazotrophicus*
IDS	indigo carmine (5,5′-indigodisulfonic acid)
Kp	*Klebsiella pneumoniae*
MoFeP	molybdenum-iron protein
MPD	2-methyl-2,4-pentanediol
RMSD	root mean square deviation
SDS-PAGE	sodium dodecyl sulfate polyacrylamide gel electrophoresis
TRIS	2-amino-2-hydroxymethylpropane-1,3-diol

Highlights

- Nitrogenase from *G. diazotrophicus* has been isolated and structurally characterized for the first time.
- The P-cluster of *G. diazotrophicus* MoFeP undergoes redox-dependent structural changes that are distinct from those of hitherto-characterized MoFeP variants from other organisms.
- The reversible ligation of the *G. diazotrophicus* P-cluster to a Tyr ligand strongly suggests the importance of hard, O-based ligands in mediating conformationally gated electron transfer (ET) in nitrogenase.

1. INTRODUCTION

1.1 Biological and Abiological Nitrogen Fixation

Conversion of atmospheric N_2 into biologically usable NH_3 is necessary for life on earth. Developing methods for enhancing plant NH_3 supply is critical for agriculture since lack of fixed nitrogen, such as NH_3, often limits crop growth (Oldroyd & Dixon, 2014; Rogers & Oldroyd, 2014). The two most important sources of NH_3 are biological nitrogen fixation by the enzyme nitrogenase and synthetic nitrogen fixation via the Haber–Bosch process (Hirsch & Mauchline, 2015).

In the Haber–Bosch process, N_2 is converted to NH_3 according to Eq. (1). This process requires high temperatures (350–550 K) to enable the activation of the inert N_2 triple bond, while high pressures (>300 atm) are concomitantly needed to drive this overall exergonic reaction forward.

$$N_2 + 3H_2 \rightarrow 2NH_3 \quad (1)$$

In contrast to the extreme conditions required in the Haber–Bosch process, biological nitrogen fixation takes place under ambient conditions, albeit at the expense of 16 ATP molecules in each catalytic cycle (Eq. 2).

$$N_2 + 8H^+ + 8e^- + 16ATP \rightarrow 2NH_3 + H_2 + 16ADP + 16P_i \qquad (2)$$

To overcome the high kinetic and thermodynamic stability of N_2, nitrogenase employs an exquisitely complex, but incompletely understood choreography of electron transfer (ET) and proton transfer (PT) processes.

Mo-containing nitrogenase is the most widely distributed form of this enzyme (Fig. 1A) (Dos Santos, Fang, Mason, Setubal, & Dixon, 2012). It consists of two protein components, the molybdenum-iron protein (MoFeP) and the iron protein (FeP). MoFeP is an $(\alpha\beta)_2$ dimer of dimers and contains two unique metal clusters, the catalytic iron-molybdenum cofactor FeMoco, a [7Fe:9S:1Mo:1C] cluster, and the P-cluster with the composition of [8Fe:7S]. FeP is a γ_2 homodimer harboring a [4Fe:4S] cluster at the dimer interface and two ATP-binding sites (Rees et al., 2005; Seefeldt, Hoffman, & Dean, 2009) (Fig. 1).

As shown in Eq. (2), each enzymatic turnover reaction by nitrogenase is an $8e^-$ process. These electrons are delivered one at a time to MoFeP by FeP, with two ATP molecules consumed by FeP for each electron transferred (Katz, Owens, & Tezcan, 2016; Seefeldt et al., 2009). FeP is the only known biological agent that can reduce MoFeP and activate it for catalysis.

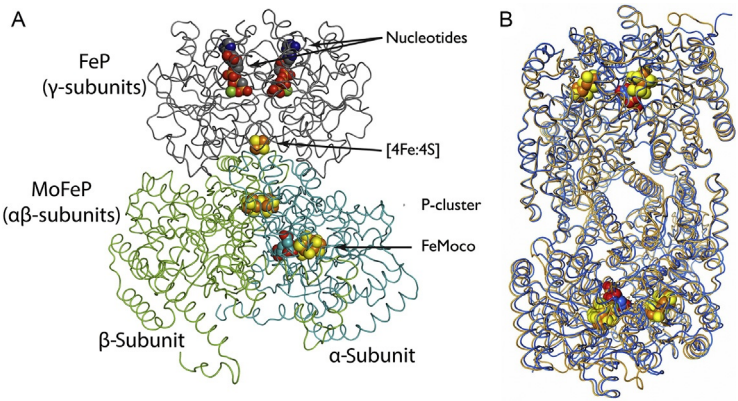

Fig. 1 (A) Structure of nitrogenase. For simplicity, only one half of the $(\alpha\beta)_2(\gamma_2)_2$ complex is shown. (B) Structural alignment of the entire $(\alpha\beta)_2$ MoFeP of *A. vinelandii* (*orange*) with that of *G. diazotrophicus* (*blue*), illustrating their structural similarity. Metal clusters and bound nucleotides are shown as *spheres*.

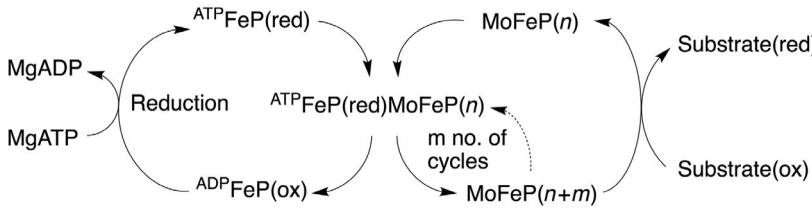

Fig. 2 Model for electron transfer and ATP hydrolysis during nitrogenase turnover. The number of cycles depends on the substrate, where $m = 8$ for N_2 and $m = 2$ for C_2H_2 and H^+. The value (n) refers to the number of electrons accumulated on FeMoco.

In turn, MoFeP is the only protein that can support ATP hydrolysis by FeP. These observations underscore the importance of specific ATP-dependent interactions between these two proteins and imply the presence of conformationally gated redox events (see Sections 1.2 and 1.3). Electrons donated by FeP are first received by the P-cluster and then relayed to FeMoco, which reduces substrates in a stepwise fashion (Fig. 2) (Hoffman, Lukoyanov, Yang, Dean, & Seefeldt, 2014; Katz et al., 2016; Lowe & Thorneley, 1984; Seefeldt et al., 2009; Wilson, Nyborg, & Watt, 2001).

1.2 Evidence for Gated-ET in Nitrogenase

Alongside the enigmatic process of N_2 reduction by FeMoco, the mechanism of ATP-driven ET events within the FeP–MoFeP complex remains one of the key unanswered questions in biological nitrogen fixation. While the structural basis for how MoFeP docking activates ATP hydrolysis by FeP is relatively well understood (Rees et al., 2005; Schindelin, Kisker, Schlessman, Howard, & Rees, 1997; Tezcan et al., 2005) (Section 1.3), the mechanism of how FeP induces conformational changes within in MoFeP is not (Section 2). Compared to other biological redox systems, FeP and MoFeP possess several distinguishing features. First, FeP differs from common electron shuttles such as flavodoxins, ferredoxins, and cytochromes by its large size and in its requirement to bind and hydrolyze ATP during ET. ATP-dependent docking interactions between FeP and MoFeP involve the formation of unusually large interfaces (Rees et al., 2005; Tezcan et al., 2005), which are more typical of permanent rather than transient protein complexes. Because of these extensive interactions, FeP dissociates from MoFeP very slowly, with an estimated rate of 6–10 s^{-1} (Lowe & Thorneley, 1984; Owens, Katz, Carter, Luca, & Tezcan, 2015; Wilson et al., 2001). It is postulated that the unusually long lifetime of the FeP–MoFeP complex may be necessary for the orchestration of gated redox events within MoFeP

(Tezcan, Kaiser, Howard, & Rees, 2015). Several other lines of evidence support conformationally controlled ET within the nitrogenase complex (Hoffman et al., 2014; Katz et al., 2016; Seefeldt et al., 2009):

(1) The rate of ET between FeP and MoFeP is dependent on the osmolarity of the solution, implying a conformational rearrangement of the FeP–MoFeP complex is required prior to interprotein ET (Danyal, Mayweather, Dean, Seefeldt, & Hoffman, 2010).

(2) The order of ET appears to be (i) slow transfer between P-cluster and FeMoco and (ii) rapid "backfill" from the P-cluster to the FeP [4Fe:4S] (Danyal, Dean, Hoffman, & Seefeldt, 2011), suggesting that the conformational gating likely involves ET from P-cluster to FeMoco.

(3) Potent, low-potential photosensitizers, placed in close proximity to P-cluster, are not able to support efficient catalysis when illuminated with light, likely due to the fact that MoFeP conformations populated during ET events in catalysis cannot be accessed in absence of FeP (Roth, Nguyen, & Tezcan, 2010; Roth & Tezcan, 2012).

These combined findings paint a picture in which reduced, ATP-bound FeP binds MoFeP, and induces conformational changes within MoFeP to activate ET between P-cluster and FeMoco (Hoffman et al., 2014; Katz et al., 2016).

1.3 Structural Dynamics of the FeP–MoFeP Complex

The crystal structures of several FeP–MoFeP complexes (from *Azotobacter vinelandii*) have been obtained under conditions relevant for ATP hydrolysis and catalytic turnover (Fig. 3) (Rees et al., 2005; Tezcan et al., 2005). These structures reveal that FeP adopts at least three distinct, nucleotide-state-dependent docking geometries (DG) (Fig. 3). In DG1, FeP largely docks with the β-subunit surface of MoFeP ("Encounter complex" in Fig. 3) (Owens et al., 2015; Willing, Georgiadis, Rees, & Howard, 1989; Willing & Howard, 1990), forming a complex that is stabilized predominantly by electrostatic interactions between negatively charged FeP residues γ110–112, and positively charged MoFeP residues β399–401 (Owens et al., 2015; Tezcan et al., 2005). In this geometry, the [4Fe:4S] of FeP is positioned >20 Å away from the P-cluster, suggesting that this conformation is not active for interprotein ET. At the same time, several lines of evidence suggest that the DG1 complex is a functionally relevant initial encounter complex whose mechanistic role is to increase the rate of association between FeP and MoFeP during turnover, especially when FeP/MoFeP

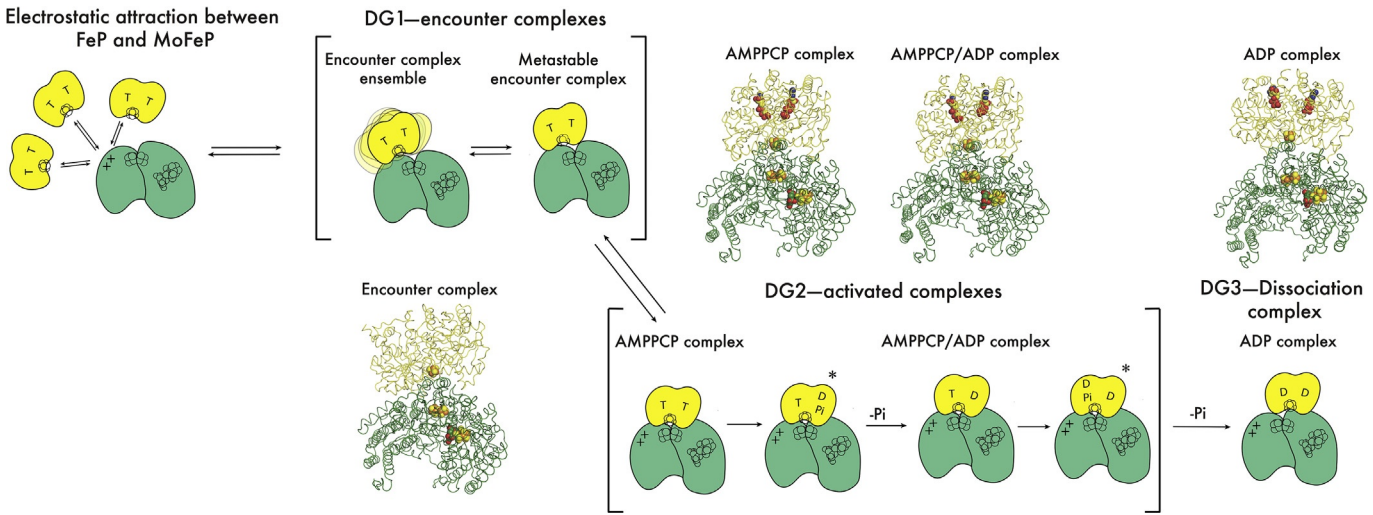

Fig. 3 Proposed scheme for nitrogenase turnover depicting ATP-dependent FeP–MoFeP interactions populated during turnover, where *T* represents ATP and D represents ADP. Conformations marked with an * are likely substrates, but have not yet been experimentally observed. The structures of known turnover intermediates are depicted as *cartoons*.

ratios are low (Owens et al., 2015; Ubbink, 2009). Indeed, elimination of favorable H-bonding and electrostatic interactions between FeP and MoFeP through point mutations such as βLys400Glu and βArg401Glu leads to considerable reduction of the catalytic activity of MoFeP (Owens et al., 2015).

DG2 represents the ATP-activated state of the nitrogenase complex and has been obtained in the presence of the nonhydrolyzable ATP analog AMPPCP or ADP·AlF_4^-, a transition-state analog for ATP hydrolysis (Fig. 3). In DG2, FeP is centrally located atop the αβ-interface surface of MoFeP, allowing the [4Fe:4S] to approach the P-cluster as closely as physically possible, yielding an ET-conducive distance of ~15 Å (Chiu et al., 2001; Schindelin et al., 1997; Tezcan et al., 2005). At the same time, FeP adopts a compact structure (particularly in the ADP·AlF_4^--bound form) that enables residues on each FeP subunit to extend across the dimer interface to participate in the hydrolysis of the bound nucleotide in the adjacent subunit. In DG2, the interface between FeP and MoFeP is particularly large (>3700 $Å^2$), which allows the FeP to undergo nucleotide-state-dependent conformational changes while retaining its central position on the MoFeP surface. Interestingly, one of the crystallographically characterized DG2 complexes is obtained in the presence of equimolar AMPPCP and ADP, with the two nucleotides bound asymmetrically by the FeP subunits ("AMPPCP/ADP complex" in Fig. 3) (Tezcan et al., 2015). This binding mode suggests that ATP hydrolysis and phosphate release within DG2 may proceed by a stepwise, rather than a concerted mechanism. Such a stepwise mechanism could be expected to prolong the lifetime of the activated FeP–MoFeP complex and, in turn, could orchestrate the sequence of intracomplex ET required for substrate reduction through the associated Fe-protein conformational changes (Spatzal, Perez, Einsle, Howard, & Rees, 2014).

Finally, DG3 is obtained in the presence of ADP and may represent a FeP–MoFeP conformation that is populated after ET and ATP hydrolysis have taken place within DG2 (ADP complex in Fig. 3) (Tezcan et al., 2005). In DG3, the ADP-bound FeP is found in a relaxed conformation typical of uncomplexed FeP variants and interacts primarily with the α-subunit surface of MoFeP. Like in the DG1 complex, the distance of >20 Å between the [4Fe:4S] cluster and the P-cluster is prohibitively long for ET. The mechanistic relevance of DG3 has yet to be probed experimentally through structure/function studies.

Taken together, these crystallographic snapshots suggest that FeP explores an unusually large conformational space along the MoFeP surface

during ATP hydrolysis, whereby distinct docking geometries are selectively populated, depending on the FeP nucleotide state. This allows the distance between the [4Fe:4S] and the P-clusters to be directly coupled to the nucleotide state, providing a way for actively modulating electron flow in nitrogenase. Interestingly, the correlation between the nucleotide state and the docking positions of FeP suggests that irreversible ATP hydrolysis may serve as a ratchet that provides directionality to protein–protein interactions, much in the same way that ATP hydrolysis ensures directed motion in proteins such as AAA^+ domains (Hanson & Whiteheart, 2005; Rappas, Bose, & Zhang, 2007) and helicase (Enemark & Joshua-Tor, 2008). Yet, none of the FeP–MoFeP complex structures offer any clues about the nature of the proposed redox-gating mechanism *within* MoFeP that could control ET between the P-cluster and FeMoco: in these complexes, MoFeP displays no structural changes near the P-cluster, FeMoco, or the intervening region between these clusters suggestive of a gating process.

1.4 Redox-Dependent Structural Changes in the P-Cluster of *A. vinelandii* MoFe Protein

A survey of all available MoFeP crystal structures (uncomplexed or complexed with FeP) reveals that the only notable conformational change observed on the ET pathway to FeMoco is on the P-cluster itself. It was established that the dithionite (DT)-reduced, all-ferrous P-cluster (P^N) could be reversibly oxidized by one and two electrons to P^{+1} and P^{OX} states, respectively (Chan, Christiansen, Dean, & Seefeldt, 1999; Igarashi & Seefeldt, 2003; Seefeldt et al., 2009). As demonstrated by a crystal structure of the *A. vinelandii* MoFeP (*Av*-MoFeP) (Peters et al., 1997), the oxidation of the P-cluster leads to a dramatic structural rearrangement: in the P^N state, the P-cluster can be viewed as a fusion of two closed [4Fe:4S] cubane architectures joined by a shared hexacoordinate sulfide, S1 (Fig. 4). In the P^{OX} state, one of the cubane units opens up, whereby Fe5 bonds to the backbone amide N of *Av*-αCys88, Fe6 ligates to *Av*-βSer188, and Fe5 and Fe6 dissociate from S1. Since both the α-Cys88 backbone N and the β-Ser188 hydroxyl group likely have to be deprotonated to coordinate Fe ions, they would stabilize the P-cluster in an oxidized state, thus lowering its reduction potential and enabling it to deliver electrons to FeMoco. Therefore, any structural perturbation induced by FeP–MoFeP association that favors ligation by *Av*-βSer188 and the *Av*-αCys88 backbone N would provide a basis for the conformational redox gating in nitrogenase.

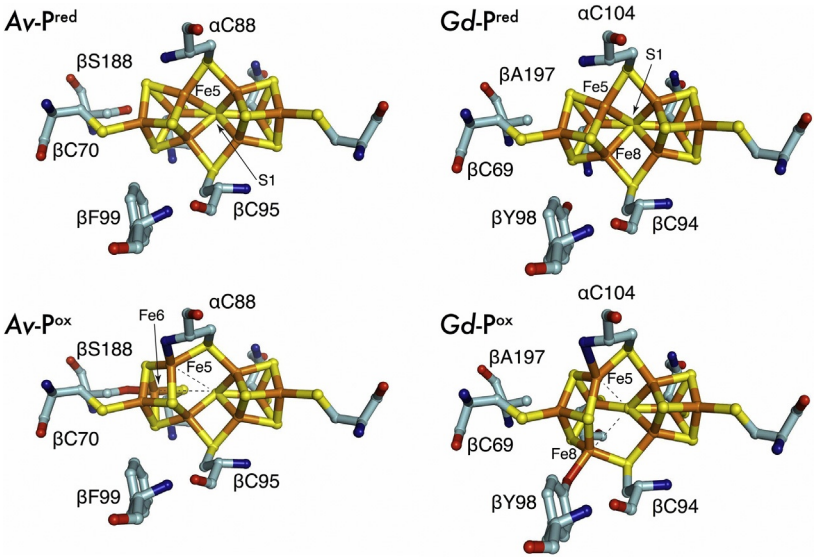

Fig. 4 Redox-dependent structural changes in *Av*- and *Gd*-MoFeP. The *dashed lines* in P^{OX} highlight bonds to the central sulfide S1 that are broken upon oxidation.

To determine if redox-dependent structural changes in the P-cluster are conserved, and thus likely to be important, we searched genomic databases and literature to find nitrogenases that showed sequence variations in residues that are proximal to the P-cluster, in particular positions equivalent to *Av*-βSer188. We limited our search to organisms with fully sequenced genomes and only considered bacterial species that could be readily cultured in a laboratory. As described later, we concluded that the diazotroph *Gluconacetobacter diazotrophicus* (*Gd*) represented a promising model organism for studying nitrogenase.

1.5 Redox-Dependent Structural Changes in the P-Cluster of *G. diazotrophicus* MoFe Protein

Most of our structural and mechanistic understanding on enzymatic nitrogen fixation has been obtained through the study of nitrogenases from a small number of diazotrophic bacteria: *A. vinelandii*, *Klebsiella pneumoniae* (*Kp*), and *Clostridium pasteurianum* (*Cp*). *A. vinelandii* and *K. pneumoniae* are closely related γ-proteobacteria and express group 1 nitrogenases (Howard, Kechris, Rees, & Glazer, 2013; Raymond, Siefert, Staples, & Blankenship, 2004) that are structurally and functionally very similar to

one another (Duyvis, Wassink, & Haaker, 1996, 1998; Einsle et al., 2002; Lowe & Thorneley, 1984; Mayer, Lawson, Gormal, Roe, & Smith, 1999; Thorneley & Lowe, 1983; Wilson et al., 2001). *Cp*-nitrogenase is structurally slightly dissimilar in the α-subunit (Zhang, Morrison, Kaiser, & Rees, 2015) and is classified as a group 2 nitrogenase (Howard et al., 2013; Raymond et al., 2004). Nevertheless, these three structurally well-characterized nitrogenases feature the same cofactor architecture and there is little sequence or structural variability in functionally critical regions of the enzyme. To gain information on the conformational gating mechanism, we decided to investigate a nitrogenase with sequence differences compared to nitrogenase from the aforementioned species, namely, *Gd*-nitrogenase.

G. diazotrophicus harbors a group 1 nitrogenase like *Av*-nitrogenase (Howard et al., 2013). *Gd*- and *Av*-nitrogenases share 60% sequence identity. However, *Gd*-nitrogenase exhibits key amino acid sequence differences surrounding the P-cluster. *Gd*-MoFeP features an Ala (*Gd*-βAla187) at the equivalent position to *Av*-βSer188 (Table 1) and a Tyr residue at the position equivalent to *Av*-βPhe99 (*Gd*-βTyr98). Interestingly, an analysis of nitrogenase sequences indicates that in the great majority of type 1 nitrogenases, the aforementioned amino acid pairs Ser/Phe and Ala/Tyr are covariant (Howard et al., 2013): if MoFeP has a Ser in the first position, it features a Phe in the second. If an organism has an Ala in the first position, it has a Tyr in the second.

To investigate whether this two-position covariance has a functional significance and if *Gd*-MoFeP P-cluster can undergo similar redox-dependent structural changes as its *A. vinelandii* counterpart, we expressed and isolated *Gd*-MoFeP protein and solved its crystal structure in P^N and P^{ox} states at 1.8 and 2.6 Å resolution, respectively (Owens, Katz, Carter, Oswald, & Tezcan,

Table 1 Sequence Alignment of *Av*-, *Kp*-, *Cp*-, *Gd*-MoFeP Illustrating Sequence Differences Surrounding the P-Cluster

	***Av*-β185–190**	***Av*-β95–100**
A. vinelandii	HTP*S*FV	CVAY*F*R
K. pneumoniae	HTPSFI	CVAY*F*R
C. pasteurianum	NTPSYV	CCCY*H*R
G. diazotrophicus	HTP*A*FV	CVAY*Y*R

2016). As expected from their high sequence homologies, the overall architecture of *Gd*-MoFeP is very similar to that of *Av*-MoFeP with an RMSD of 0.7 Å over all αC atoms (Fig. 1B). The coordination and the outer-sphere environments of FeMoco are identical to one another in both species. Furthermore, in the P^N state, *Av*-P-cluster and *Gd*-P-cluster are fully superimposable (Fig. 4).

In contrast, the P^{ox} form of the *Gd*-MoFeP P-cluster displays striking differences from its *Av*-MoFeP counterpart, as shown in Fig. 4 and Table 2. Analogous to structural changes observed in *Av*-MoFeP, Fe5 becomes ligated to the backbone N of *Gd*-αCys104 and dissociates from the central S1 upon P-cluster oxidation. However, Ser, which coordinates Fe6 in *Av*-, *Kp*-, and *Cp*-MoFeP, is replaced by Ala in *Gd*-MoFeP. Instead, Fe8 now coordinates the O atom of the *Gd*-βTyr98 side chain. Tyr-ligated Fe8 also fully dissociates from S1 like the Ser-coordinated Fe6 in other species. Thus, while $2e^-$ oxidation of the P-clusters in both *Gd*- and *Av*-MoFeP yields an opened 4Fe–3S unit with two O- and N-based ligands, the mechanism by which this is achieved is distinct in these species.

While ligation of a Ser or Tyr to an FeS cluster is rare (Nicolet, Rohac, Martin, & Fontecilla-Camps, 2013), the role of an O-based ligand as a redox switch for an FeS-cluster can be readily explained. Coordination by the singly anionic tyrosinate (Tyr^-) or serinate (Ser^-) side chains would decrease the reduction potential of the P-cluster to induce ET to FeMoco, much like a cysteinate (Cys^-) ligand. However, unlike the borderline soft Cys^- ligand, the coordination of the hard Tyr^- and Ser^- ligands to an FeS-cluster would be highly dependent on whether the Fe center that they coordinate to is in the +3 (hard, favored) or +2 (borderline soft, disfavored) oxidation state. In other words, while Cys^- is a good permanent ligand that can stably anchor an Fe–S cluster in all oxidation states, Tyr^- and Ser^- are conditionally labile ligands that are well suited for reversible redox switching.

Table 2 Changes in Coordination Distances of the P-Cluster Upon Oxidation ($P^N \rightarrow P^{OX}$) in *A. vinelandii* and *G. diazotrophicus*

	d **(S1–Fe6/Fe8) (Å)**	***d*** **($O^{Ser/Tyr}$–Fe6/Fe8) (Å)**	***d*** **(N^{Cys}–Fe5) (Å)**
Av-MoFeP	2.5 → 4.0	3.4 → 1.9	3.4 → 2.1
Cp-MoFeP	2.4 → 3.6	3.2 → 2.0	3.3 → 2.3
Kp-MoFeP	2.4 → 3.8	3.6 → 2.2	3.4 → 2.2
Gd-MoFeP	2.5 → 3.4	3.6 → 2.1	3.4 → 2.6

Our findings strongly suggest that redox-dependent structural changes at P-cluster are conserved and therefore likely relevant for nitrogenase function. Furthermore, the fact that P-cluster can cycle between the P^N and P^{OX} state through the engagement of conserved structural features hints at the possibility that it may be capable of transferring two electrons to FeMoco during catalytic turnover. Such $2e^-$ transfer steps between P-cluster and FeMoco may help minimize wasteful H^+ reduction during turnover by increasing the electron flux to FeMoco (Katz et al., 2016; Owens et al., 2016). Nevertheless, the functional importance of the P^{OX} state has yet to be experimentally established, as only P^N and P^{+1} have been detected under catalytic turnover conditions (Igarashi & Seefeldt, 2003; Lanzilotta, Christiansen, Dean, & Seefeldt, 1998). Likewise, the mechanism by which FeP–MoFeP interactions can induce conformational changes in the P-cluster at a distance of >15 Å and modulate its coordination-dependent redox equilibria also remains an exciting topic for future studies.

2. MATERIALS AND METHODS

The methods presented herein describe how to efficiently culture *G. diazotrophicus* in large scale for expression of *Gd*-nitrogenase component proteins. These procedures are based on protocols first introduced by Fisher and Newton (2005), and then adopted and modified by us (Owens et al., 2016). For more detailed information on factors influencing *G. diazotrophicus* growth, readers are directed to Reis and Döbereiner (1998), Flores-Encarnacion et al. (1999), and Tejera, Ortega, Rodes, and Lluch (2004). We furthermore present methods on the crystallographic and spectroscopic (EPR) characterization of *Gd*-MoFeP.

2.1 *G. diazotrophicus* as a Model Nitrogen-Fixing Organism

G. diazotrophicus is a gram-negative α-proteobacterium that was first isolated from sugarcane in Brazil (Cavalcante & Dobereiner, 1988). It is an endophyte that establishes symbiosis with its host by infecting the host plant's roots where it colonizes intercellular spaces (Saravanan, Madhaiyan, Osborne, Thangaraju, & Sa, 2008). Unlike the other nitrogenase model organisms *A. vinelandii*, *K. pneumoniae*, and *C. pasteurianum*, *G. diazotrophicus* is an agriculturally important species due to its plant growth enhancing properties which have been documented in several crops, including sugar cane, coffee, and rice (Pedraza, 2008; Saravanan et al., 2008; Sevilla, Burris,

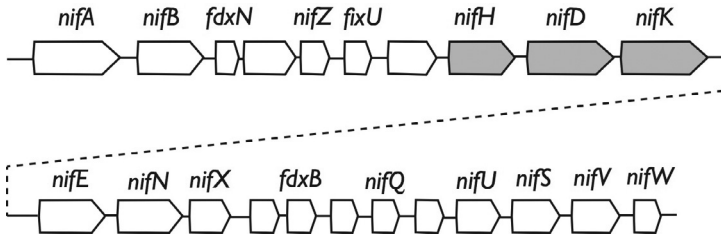

Fig. 5 *Nif* operon of *G. diazotrophicus*. *NifH* represents FeP, *nifD*, the α-subunit of MoFeP and *nifK* the β-subunit. For clarity, *nif* genes downstream of nifW (*fixA—modD*) have been omitted.

Gunapala, & Kennedy, 2001). The economic potential of *G. diazotrophicus* is highlighted by the fact that it is often included in "biofertilizer" products, which contain a variety of plant growth promoting, beneficial bacteria.

The entire genome *G. diazotrophicus* has been sequenced and it indicates that the organization of its nitrogen fixing genes resembles that of other proteobacteria such as *A. vinelandii* (Bertalan et al., 2009; Giongo, Tyler, Zipperer, & Triplett, 2010; Lee, Reth, Meletzus, Sevilla, & Kennedy, 2000). *Gd*-nitrogenase is part of the *nif* operon, which contains the genes for FeP, both MoFeP subunits, and several accessory proteins (Fig. 5).

2.2 Equipment and Reagents

2.2.1 Major Equipment and Instruments Needed

Anaerobic chamber (e.g., Coy glovebag)
Crystal trays and crystallography tools
Liquid nitrogen
Fast protein liquid chromatography (FPLC) workstation
Gas chromatograph with flame ionization detector (FID)
Gastight syringes (multiple sizes from 0.025 to 1 mL)
Large capacity shaker (e.g., Amerex 767, New Brunswick Excella E25)
Large capacity Erlenmeyer (6 L) or Fernbach (2.8 L) flasks
Large round bottom flasks (1.5–3 L) to hold buffers with adaptors to connect to Schlenk line and FPLC
Microfluidizer
Pear-shaped flasks (5, 10, 200, and 500 mL) for loading protein onto FPLC
Schlenk line
Stoppered 10 or 14-mL glass serum vials (Wheaton)

2.2.2 Reagents Required for the Growth of G. diazotrophicus

Metal salts

$CaCl_2 \cdot 2H_2O$
$FeSO_4 \cdot 7H_2O$
$MgSO_4 \cdot 7H_2O$
$Na_2MoO_4 \cdot 2H_2O$

Sugar

Glucose
Sucrose

Buffer

K_2HPO_4
KH_2PO_4

Nitrogen source

$(NH_4)_2SO_4$
NH_4Cl

C2 media components

Peptone
NaCl
Yeast extract
Agar (for solid media only)

Indicators

Bromophenol blue
Bromothymol blue

2.2.3 Reagents Required for Nitrogenase Purification, Enzymatic Assays, and Crystallization

Nitrogenase purification

NaCl
Tris base
Sodium dithionite (DT)

Enzymatic assays

ATP (as Na_2ATP)
Creatine phosphate
Creatine phosphatase
Glacial acetic acid to quench reaction
$MgCl_2$

Concentration measurement

Urea
2,2-Bipyridine

Crystallography

2-Methyl-2,4-pentanediol (MPD)
Indigo sulfonate (indigo carmine, IDS)
Sodium cacodylate
Spermine
Zwittergent (a zwitterionic detergent)

2.3 Growth Media for *G. diazotrophicus* Cultures

G. diazotrophicus is grown in LGI media for nitrogenase expression. To maintain cell stocks, LGI, LGIP, or C2 media can be used (Figs. 6 and 7).

(1) LGI contains 10% glucose 0.14 m*M* $CaCl_2$, 0.81 m*M* $MgSO_4$, 0.036 m*M* $FeSO_4$, 0.008 m*M* $NaMo_2O_4$, 0.5 m*M* $(NH_4)_2SO_4$ or 1 m*M* NH_4Cl, 10 m*M* KPO_4 (pH 6.0).

(2) LGIP can be used as an alternative to LGI for cell culture maintenance. LGIP uses the same recipe as LGI with the exception that sucrose is used instead of glucose. We do not recommend using LGIP for nitrogenase expression since the amount of nitrogenase produced is higher when using LGI, an observation that can be attributed to the higher respiration rate of *G. diazotrophicus* when glucose is used as the carbon source (Tejera et al., 2004).

(3) To make solid media, agar is added to a concentration of 12 g/L.

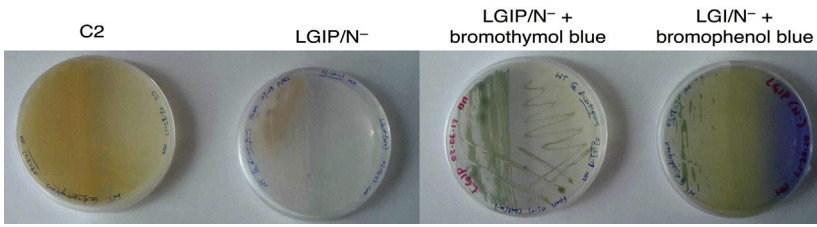

Fig. 6 *G. diazotrophicus* grown on different types of solid media. *G. diazotrophicus* grows to highest density on rich media (C2) compared to minimal, NH_4^+-free media (LGIP and LGI). Both bromothymol blue and bromophenol blue can be used to better visualize bacteria. Bromothymol blue is taken up by the bacteria, where it is *green* at neutral pH. This provides contrast to media, where bromothymol blue is almost clear under acidic conditions. Bromophenol is *blue-green* when taken up by *G. diazotrophicus*. As *G. diazotrophicus* acidifies the surrounding media during growth, bromophenol blue in the media changes color from *blue* to *yellow*. This color change is useful for visualizing the extent of bacterial growth. When grown to full density, the LGI plate containing bromophenol blue should be almost completely *yellow*.

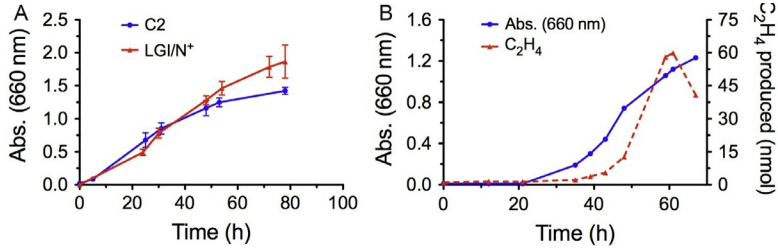

Fig. 7 (A) Growth curves for *G. diazotrophicus* grown in rich C2 and LGI/N^+ (10 m*M* NH_4^+) media. (B) Growth curves for *G. diazotrophicus* grown under N_2-fixing conditions. The growth medium contains 1 m*M* NH_4^+. Nitrogenase expression is monitored by measuring reduction of the alternative substrate C_2H_2 to C_2H_4. Nitrogenase expression starts in mid-exponential phase (≥40 h) when NH_4^+ originally present in the medium is depleted. It is important to continuously monitor C_2H_4 production since MoFeP expression decreases slightly once intracellular NH_4^+ levels reach homostasis (Hamilton et al., 2011). Note that the different durations of the lag phases in (A) and (B) are due to the fact that different amounts of starter cultures were used for inoculation.

(4) We observed that while growing *G. diazotrophicus* in absence of any fixed nitrogen is possible on solid media (Fig. 6), doing so in liquid media results in impractically long lag phases. Therefore, 0.5 m*M* $(NH_4)_2SO_4$ or 1 m*M* NH_4Cl is added to liquid media (Fig. 7). If high-level nitrogenase expression is not the primary goal, more NH_4^+ (up to a concentration of 10 m*M*) can be added to increase the bacterial growth rate (Fig. 7).

(5) C2 media is a rich media, made by mixing 10 g peptone, 15 g glucose, 5 g NaCl, and 5 g yeast extract per liter and adjusting the pH of the media to 6.0 with acetic acid.

For the improved visualization of cell colonies on solid media, pH indicators (bromothymol blue or bromophenol blue) can be added to the media. During growth, *G. diazotrophicus* secretes organic acids, which cause the pH of growth media to decrease from 6.0 to 2.5–3.5 (Fig. 6) and a concomitant change in indicator color. Per liter of solid media, 5 mL of indicator is added from a 0.5% solution dissolved in 0.5 N KOH.

2.4 Freezer Stocks of *G. diazotrophicus*

(1) Starting with a single colony from C2 or an LGI agar plate, start a 100-mL C2 or LGI/N^+ (10 m*M* NH_4^+) culture in a 500-mL Erlenmeyer flask. Cultures are grown in an orbital shaker, with a speed of 200 rpm at 30°C.

(2) To make a freezer stock, grow *G. diazotrophicus* to late exponential phase such that OD_{660nm} is ca. 1.0.

(3) Spin down the cells, at $2000 \times g$ for 15 min.
(4) Resuspend the cells gently in 1/20th of the original volume in LGI supplemented with 20 mg/L yeast extract and 20% (v/v) glycerol.
(5) Freeze the cells in liquid N_2 and store at −80°C.

2.5 Nitrogenase Expression in *G. diazotrophicus*

2.5.1 General Growth Considerations

To date, no heterologous expression system exists to produce nitrogenase in high yield. Although it is possible to express both FeP and MoFeP in *Escherichia coli* (Buren et al., 2017) and MoFeP in yeast (Wang et al., 2013), expression levels are very low and not suitable for large scale biochemical and structural investigations. Therefore, nitrogenase is produced in the native host organism under the control of its native promoter. To induce nitrogenase expression in *G. diazotrophicus*, cells are cultured in LGI media containing 1 m*M* NH_4^+, which is added to allow *G. diazotrophicus* to grow rapidly until mid-exponential phase, where the bacteria run out of fixed nitrogen. After NH_4^+ is depleted, *G. diazotrophicus* starts transcribing the *nif* operon and reducing N_2 (Fig. 7) (Hamilton et al., 2011).

To obtain sufficient quantities of protein required for protein crystallography, we found that growth of multiple medium-sized batches of *G. diazotrophicus* cultures (10 − 12 L) in 6 L Erlenmeyer or 2.8 L Fernbach flasks works quite well. While it was reported that large-volume fermenters can be used for nitrogenase expression in *G. diazotrophicus* (Fisher & Newton, 2005), we found that the protein yields from flask-grown cultures are superior to those of grown in fermenters (60 L, in our case).

2.5.2 Factors Affecting Nitrogenase Expression in G. diazotrophicus

The levels of nitrogenase expression in *G. diazotrophicus* are affected by aeration, the type of carbon source, and the concentration of sugar (carbon source) in the medium (Flores-Encarnacion et al., 1999; Reis & Döbereiner, 1998). To maximize the yield of *Gd*-nitrogenase, bacteria are grown in LGI media containing 10% (w/v) glucose. *G. diazotrophicus* is an obligate aerobe, and high aeration rates are necessary to meet the bacterium's respiratory needs under N_2-fixing conditions (Flores-Encarnacion et al., 1999). Optimal aeration conditions for nitrogenase expression in *G. diazotrophicus* entail agitation at 200 rpm in an orbital shaker, with Erlenmeyer flasks containing 0.4 L of media per liter flask volume, or Fernbach flasks filled with 0.55 L of media per liter flask volume. We found that lower or higher rates of aeration negatively affects nitrogenase yields.

(1) Starting with a freezer stock, prepare a 200-mL LGI starter culture and grow the culture until the cells reach late exponential or early stationary phase. The cell density at this point should be between 1.5 and 2 at 660 nm.
(2) To start large-scale growth, inoculate fresh LGI with 20 mL/L of starter culture.
(3) Monitor cell growth by measuring OD_{660nm} and measure nitrogenase expression by observing C_2H_2 reduction (Fig. 7 and Section 2.5.3).
(4) Nitrogenase expression is first observed after 2–3 days when OD_{660nm} ranges between 1 and 1.5.
(5) Peak nitrogenase activity is approximately 40–80 nmol C_2H_4 per 1 mL of cell culture (Fig. 7).
(6) After detecting high levels of C_2H_4, grow *G. diazotrophicus* for an additional 2–4 h. During this period, monitor C_2H_2 reduction every 1 h.
(7) Harvest *G. diazotrophicus* by centrifugation at $2000 \times g$ for 15 min. Typical *G. diazotrophicus* yield is 2.5 g per liter of LGI.
(8) The cell pellet may be stored indefinitely at −80°C.

2.5.3 Monitoring Nitrogenase Activity in Whole Cells

(1) Place 1 mL of cells in a stoppered serum vial and add C_2H_2 to a pressure of 0.072 atm. This step is done by transferring C_2H_2 from a previously degassed round bottom flask filled with C_2H_2 to the stoppered vial filled using a gastight syringe.
(2) Place the cells in a shaking water bath set to 30°C, and incubate them for 10–15 min.
(3) *G. diazotrophicus* expressing nitrogenase reduces C_2H_2 to C_2H_4. C_2H_2 and C_2H_4 can be separated by GC on an alumina column and detected using an FID detector.

2.6 Buffers and Solutions for *G. diazotrophicus* Lysis and Nitrogenase Purification

Protein purification	
Resupension, lysis, and wash buffer (Buffer R)	50 m*M* Tris (pH 8), 100 m*M* NaCl, 5 m*M* DT
Elution buffer (Buffer E)	50 m*M* Tris (pH 8), 500 m*M* NaCl, 5 m*M* DT
Gel-filtration buffer (Buffer GF)	50 m*M* Tris (pH 8), 500 m*M* NaCl, 5 m*M* DT

Continued

Activity assay	
Buffer A	50 m*M* Tris (pH 8), 5 m*M* $MgCl_2$, 5 m*M* ATP, 30 m*M* creatine phosphate, 0.125 mg/mL creatine phosphatase
Buffer B	0.5 *M* Tris base
Buffer C	50 m*M* Tris (pH 8), 500 m*M* NaCl
Protein concentration measurement	
Urea	8 *M*
Bipyridine	100 m*M* in 50% glacial acetic acid

2.7 Isolation and Purification of *G. diazotrophicus* Nitrogenase

2.7.1 General Procedures for Working With Nitrogenase

Nitrogenase component proteins are highly air sensitive. *Gd*-nitrogenase is manipulated using anaerobic methods on a Schlenk line and in an anaerobic chamber at O_2 levels below 5 ppm. All buffers and equipment are degassed and, unless specifically indicated, DT is added to a concentration of 5 m*M* to maintain a reducing environment.

2.7.2 Lysis

(1) Thaw *G. diazotrophicus* on ice.

(2) Resuspend *G. diazotrophicus* in chilled Buffer R. Add 3 mL of buffer per gram of cells. It is important to keep all solutions cool during lysis to avoid heat denaturation of *Gd*-FeP. Prior to lysis, add DT to a final concentration of 5 m*M* to the resuspended cell pellet.

Because neither osmotic lysis methods nor sonication efficiently lyse *G. diazotrophicus* cells, we prefer using a microfluidizer. The exact protocol of cell lysis will be dependent on the specific hardware. We use an LM10 instrument fitted with an F12Y interaction chamber (Microfluidics Corporation) to lyse *G. diazotrophicus* at 16,000–18,000 psi. Typically, three passes are needed to fully lyse the entire cell pellet. To avoid oxygen damage to nitrogenase, lysis is carried out under a blanket of Ar.

(3) Place the cell lysate in an airtight centrifuge bottle equipped with a rubber septum and degas the solution for a total of 20 min on a Schlenk line by repeatedly exchanging the headspace with Ar.

(4) Clarify the cell lysate by centrifugation at 17,500 $\times g$ for 1 h. During centrifugation, the supernatant may darken slightly.
(5) After clarification, transfer the supernatant to a pear-shaped flask in an anaerobic chamber (Fig. 8A).

2.7.3 Purification

(1) Load the clarified lysate onto a DEAE column preequilibrated with anaerobic buffer R. Use ca. 7.5 mL of DEAE resin per gram of cell paste.
(2) Wash the column with fresh Buffer E until the flow through is clear.
(3) Elute *Gd*-MoFeP and *Gd*-FeP using a 100–500 m*M* linear NaCl gradient. *Gd*-MoFeP and *Gd*-FeP coelute between 250 and 300 m*M* NaCl (Fig. 8B).
(4) Determine the presence and purity of *Gd*-MoFeP and *Gd*-FeP by SDS-PAGE. *Gd*-MoFeP and *Gd*-FeP mostly coelute and there is no benefit to separating *Gd*-MoFeP and *Gd*-FeP fractions at this stage.
(5) Pool *Gd*-FeP/*Gd*-MoFeP fractions, concentrate the resulting solution to 5–10 mL in an anaerobic chamber, and load it onto a Superdex 200 gel filtration column equilibrated with anaerobic Buffer GF. The gel filtration column removes remaining impurities from *Gd*-MoFeP and *Gd*-FeP and separates the proteins from each other (Fig. 8C). The major impurity is a ferredoxin (ca. 8 kDa), which elutes after both *Gd*-nitrogenase components.
(6) Use SDS-PAGE to identify proteins contained in each collected fraction.
(7) Typical *Gd*-MoFeP yields are 2–4 mg protein per liter of cell culture (0.08–0.2 mg *Gd*-MoFeP per gram of cell pellet).
(8) Pool and concentrate the respective fractions of *Gd*-FeP and *Gd*-MoFeP and run an SDS-PAGE to evaluate the purity of the respective proteins (Fig. 8D).
(9) Measure the concentration of the respective proteins using the Bradford assay (Bradford, 1976) and by measuring the protein's respective Fe content. For the later assay, mix 10–20 μL of protein with 780–790 μL of 8 *M* urea and 100 μL of 0.1 *M* bipyridine. Let the sample incubate for 5 min and determine the Fe concentration using $\varepsilon_{522\text{nm}} = 8650\, M^{-1}\ \text{cm}^{-1}$.
(10) Purified proteins can be stored in liquid nitrogen indefinitely.

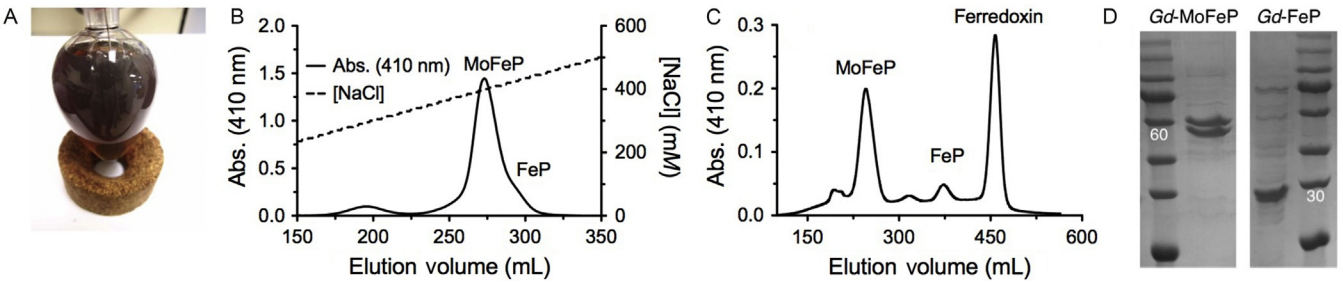

Fig. 8 (A) Clarified cell lysate collected in a pear-shaped flask. The *brown color* arises from the FeS clusters of MoFeP and FeP. (B) DEAE and (C) gel filtration chromatograms of *Gd*-nitrogenase. Note that in the ion exchange step, MoFeP and FeP coelute. We do not recommend trying to separate the nitrogenase components in this step, since they are readily separated by gel filtration chromatography at a later stage. (D) SDS-PAGE of purified *Gd*-MoFeP and *Gd*-FeP with relevant molecular weight marker bands indicated. The double band for *Gd*-MoFeP arises from the α and β subunits.

2.8 Enzymatic Activity Assays for *Gd*-Nitrogenase

The activity of *Gd*-nitrogenase is measured according to previously described protocols for C_2H_2 reduction (Fisher & Newton, 2005; Owens et al., 2015, 2016). Experiments are conducted under an Ar atmosphere in stoppered serum vials containing a buffered activity assay solution of 50 m*M* Tris (pH 8), 60 m*M* NaCl, 5 m*M* ATP, 5 m*M* $MgCl_2$, 30 m*M* creatine phosphate, 0.125 mg/mL creatine phosphokinase, and 13 m*M* DT.

(1) Mix the appropriate amounts of Buffer A and Buffer C in serum vials to make the activity assay solution. The total volume of a typical reaction in our experiments is typically ~1.1 mL. The amount of Buffer C that needs to be added to Buffer A will vary depending on the volume of *Gd*-MoFeP and *Gd*-FeP that is added in steps 5 and 6.

(2) Degas 2 mL of Buffer B in a stoppered serum vial and use it to anaerobically dissolve DT to a final concentration of 0.5 *M*.

(3) Degas the serum vials containing the activity assay solution and add DT to a final concentration of 13 m*M* using a gastight syringe.

(4) Add C_2H_2 to each serum vial to a final pressure of 0.072 atm using a gastight syringe.

(5) Add *Gd*-MoFeP, suspended in buffer C, to final concentration of 0.2 μ*M* to each serum vial using a gastight syringe.

(6) To initiate the reaction, anaerobically add increasing amounts of *Gd*-FeP, suspended in buffer C, to final concentrations ranging between 0 and 12 μ*M* using a gastight syringe.

(7) Incubate the reaction for 10 min at 30°C in a shaking water bath.

(8) Terminate the reaction by adding 0.3 mL of glacial acetic acid.

(9) C_2H_2 and C_2H_4 can be separated by GC using an alumina column and detected using an FID.

The specific C_2H_2 reduction activity of *Gd*-MoFeP ranges between 1000 and 1500 nmol mg^{-1} min^{-1}.

2.9 Electron Paramagnetic Resonance Spectroscopy of *G. diazotrophicus* MoFe Protein

Electron paramagnetic resonance (EPR) spectroscopy is a powerful method to monitor and characterize different redox states of the P-cluster and FeMoco. In the perpendicular collection mode, DT-reduced MoFeP displays signals at $g \sim 4.3$, 3.6, and 2.0, arising from the resting-state ($S = 3/2$) FeMoco (termed M^N) (Igarashi & Seefeldt, 2003). Under these conditions, the all-ferrous P-cluster (i.e., P^N) is EPR-silent in both parallel

and perpendicular modes. In the $2e^-$ oxidized P^{OX} state, the P-cluster features a diamagnetic $S \geq 3$ non-Kramers doublet with a signal at large g-values ($g = 12$ in *Av*-MoFeP, $g = 16$ in *Gd*-MoFeP) (Igarashi & Seefeldt, 2003), observable in parallel collection mode. For more information on EPR spectroscopy of nitrogenase, the reader is directed to reviews by Igarashi and Seefeldt (2003) and Danyal, Yang, and Seefeldt (2011).

(1) Set up EPR experiments using protein concentrations of ≥ 50 μ*M* in an anaerobic chamber.

(2) To generate P^N, add DT to a concentration of 5 m*M* to *Gd*-MoFeP and incubate for ≥5 min. Place the protein in an EPR tube and seal the tube.

(3) For P^{OX} samples, first remove any DT by running MoFeP over a desalting column (e.g., 10DG from Bio-Rad) prior to adding IDS. Then, add IDS to *Gd*-MoFeP a final concentration of 0.42 m*M*.

(4) Flash freeze EPR tubes containing P^N and P^{OX} samples in liquid N_2.

(5) All EPR experiments are carried out at 10 K.

(6) Collect perpendicular-mode spectra on an X-band EPR spectrometer using the following settings: microwave frequency, 9.64 GHz; modulation frequency, 100.00 Hz; modulation amplitude, 10.02; microwave power, 6.4 mW; attenuation, 15.0 dB; time constant, 81.92 ms; conversion time, 40.96 ms.

DT-reduced *Gd*-MoFeP features a signal for FeMoco in the M^N state with peaks at $g = 4.3$, 3.6, and 2.0 (Fig. 9).

(7) Collect parallel-mode spectra on an X-band EPR spectrometer using the following settings: microwave frequency, 9.36 GHz; modulation frequency, 100.00 Hz; modulation amplitude, 10.02; microwave power, 6.4 mW; attenuation, 15.0 dB; time constant, 81.92 ms; conversion time, 40.96 ms.

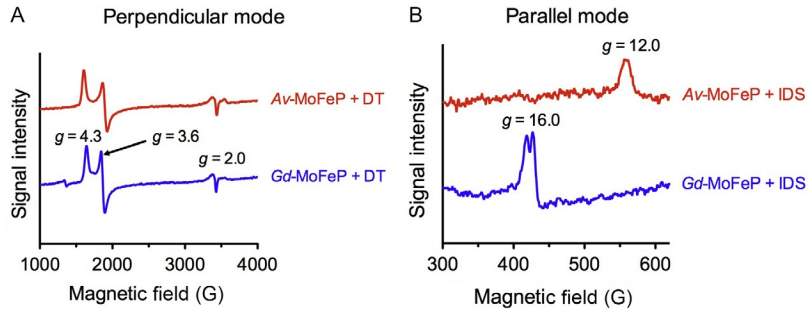

Fig. 9 EPR spectra of *Gd*-MoFeP compared to *Av*-MoFeP. The experimental conditions are described in the main text.

IDS-oxidized *Gd*-MoFeP features a signal at $g = 16.0$ in the parallel collection mode, indicative of $2e^-$ oxidized P-cluster with $S \geq 3$ (Fig. 9). In perpendicular mode, the signal of DT-reduced and IDS-oxidized *Gd*-MoFeP is identical since no change in the FeMoco oxidation state occurs (Owens et al., 2016).

(8) To obtain high signal-to-noise spectra, collect at least 20 scans per sample.

Since EPR spectroscopy is a nondestructive technique, protein can be removed from the EPR tube and used for subsequent experiments. Furthermore, redox-dependent changes in the P-cluster are reversible. MoFeP in the P^{OX} state can be reduced by addition of excess DT, and MoFeP in the P^{N} state can be oxidized by addition of excess IDS.

2.10 Crystallography of *G. diazotrophicus* MoFe Protein

2.10.1 Crystallization

Several successful methods and conditions for MoFeP crystallization have been developed. For a thorough review on nitrogenase crystallography, we direct the reader to a review by Roth and Tezcan (2011). To crystallize *Gd*-MoFeP, we chose to set up crystallization trials in a 24-well sitting drop format. The general format of the tray uses a solution of sodium 0.1 *M* cacodylate (pH 6.5), 40%–50% MPD, and 0.2–0.6 *M* NaCl.

(1) Place a stereomicroscope in the anaerobic chamber to be able to view crystals without removing the crystal trays from the chamber.

(2) Crystallization of DT-reduced *Gd*-nitrogenase: Grow crystals anaerobically using the sitting drop method with a *Gd*-MoFeP concentration of ca. 170 μ*M* (40 mg/mL). The well solution contains 45% MPD, 300 m*M* NaCl, 100 m*M* sodium cacodylate (pH 6.5), 1 m*M* spermine, 0.1% Zwittergent, and 5 m*M* DT. The drop consists of 2 μL *Gd*-MoFeP in a buffered solution of 25 m*M* Tris (pH 8), 100 m*M* NaCl, and 2 μL of well solution.

(3) Crystallization of IDS-oxidized *Gd*-nitrogenase: Remove DT from MoFeP by running the protein over a desalting column (e.g., 10DG column by Bio-Rad) or by buffer exchanging the protein at least 3× using a spin concentrator (e.g., Millipore spin-concentrator with 10 or 20 kDa molecular weight cutoff).

To obtain oxidized Gd-MoFeP crystals, 2 μL of *Gd*-MoFeP (170 μ*M*) is mixed with 2 μL of well solution containing of 50% MPD, 300 m*M* NaCl, 100 m*M* sodium cacodylate (pH 6.5), 1 m*M*

spermine, and 0.43 m*M* IDS. IDS is added from a 42 m*M* stock, which is spun at 12,000 × *g* prior to use to remove undissolved IDS.

For both reduced and oxidized *Gd*-MoFeP, the best diffracting crystals were obtained with 45%–50% MPD, however, we recommend using a broader range of MPD concentrations (40%–55% in initial screens. While the inclusion of NaCl led to the highest quality crystals, we also observed diffraction-quality crystals when NaCl was replaced with KCl. Similarly, high-quality crystals were found both in presence and absence of Zwittergent and spermine. To find best diffracting crystals, we recommend adjusting the concentration of spermine between 0 and 1 m*M* in a fine screen.

The crystal morphology is identical in both redox conditions. *Gd*-MoFeP crystals appear as rectangular rods with dimensions varying between approximately 0.04 and 0.4 mm. Crystals start to appear within 24 h, with additional crystals forming for up to 1 week.

(4) *Gd*-MoFeP crystals are harvested aerobically and flash frozen in liquid N_2. At 40%–50%, MPD itself acts as a glassing agent so no additional cryoprotectants are needed. To prevent oxygen damage during crystal harvesting, unseal only one well at a time, and complete harvesting within 5 min per tray. To further reduce oxygen damage and to keep the crystals anaerobic, harvesting can be carried out under a stream of inert gas.

2.10.2 Data Collection, Data Processing, and Structural Refinement

Diffraction experiments are carried out at a synchrotron or a home source, where the experimental strategy needs to be optimized for the respective hardware. Multiple free and commercially available indexing and integrating options are available today, including XDS (Kabsch, 2010), HKL2000 (Otwinowski & Minor, 1997), and iMosflm (Battye, Kontogiannis, Johnson, Powell, & Leslie, 2011). Aimless (Evans & Murshudov, 2013) can be used for scaling and merging, and Ctruncate (Evans & Murshudov, 2013) to convert structure factors to amplitudes.

2.10.3 Structural Refinement

The structure of *Gd*-MoFeP can be solved by molecular replacement, using the structure of *Av*-MoFeP as the search model. We recommend removing metal clusters from the search model. Phasing can be carried out using freely available software, including PhaserMR (Adams et al., 2010) and Molrep (Winn et al., 2011). The structure can be refined automatically using refmac

(Murshudov, Vagin, & Dodson, 1997), phenix.refine (Adams et al., 2010), and manually in Coot (Emsley, Lohkamp, Scott, & Cowtan, 2010).

To build the metal clusters, start with manual refinement.

(1) Open the coordinates of the P-cluster and FeMoco from an existing MoFeP structure and the coordinates of *Gd*-MoFeP in Coot (Emsley & Cowtan, 2004) and move the clusters into the corresponding regions of electron density, simultaneously using the $2F_o–F_c$ and $F_o–F_c$ maps. Then, merge the coordinates of the clusters with those of the polypeptide.

(2) After initial cluster placement, move the individual cluster atoms manually until they fit the electron density map.

Geometry constraints are necessary for automated refinement of the FeMoco and P-cluster. The respective constraint file contains coordinate and geometry information for each metal cluster. The files include values for each bond length, bond angle, and torsion (dihedral) angle in the respective cluster, as well as the maximum allowed deviation for each of the values. For both P-cluster and FeMoco, the maximum allowed deviation is 0.020 Å for bond distances, 3 degrees for bond angles, and 20 degrees for torsion angles. Making a new constraint file is necessary whenever the structure that needs to be refined differs substantially from one used to build the original constraint file. Since the structures of FeMoco and P^N in *Gd*-MoFeP closely resemble those in *Av*-MoFeP, existing constraint files originally generated for *Av*-MoFeP can be used. In this case, automated refinement will accurately place the atoms of the metal clusters into the electron density map and little additional manual refinement is needed.

The structure of P^{OX} in *Gd*-FeMoco, however, features large structural changes involving Fe6 and Fe8 that differ from *Av*-MoFeP P^{OX}. Therefore, oxidized *Gd*-MoFeP requires a new constraint file for P^{OX}. To make a new constraint file, the protein structure is first opened in Coot and the P-cluster is manually rebuilt by moving Fe and S ions until all cluster atoms fit the $2F_c–F_c$ electron density map. After fully placing the cluster, distances, bond angles, and torsion angles between cluster atoms are measured in Coot or in Pymol (Schrödinger). The values for respective distances and angles are input into a text editor according to cif format guidelines (Hall, Allen, & Brown, 1991) to create a new constraint file. Since the main difference between the structures of *Gd*-P^{OX} and *Gd*-P^N is the location of Fe5 and Fe8, we recommend using the constraint file for P^N as a template and modifying only those parameters that differ between P^{OX} and P^N. The text file can be saved as a ".cif" file that is recognized as a constraint file by refmac and phenix.refine.

3. CONCLUSION

Here, we have summarized recent studies on the ATP- and oxidation-state dependent structural dynamics of nitrogenase and the insights gained in these studies. Our investigations were greatly enriched by the examination of MoFeP from a new model organism, *G. diazotrophicus*. To afford easy access to similar investigations, we have described here methods for the isolation and characterization of *Gd*-MoFeP. We hope that the relatively straightforward expression, purification, and crystallization protocols for *Gd*-MoFeP will encourage researchers to include this variant in their mechanistic investigations on biological nitrogen fixation, and rekindle the lost interest in the study of nitrogenases from different diazotrophic bacteria (Brendt, Lowe, & Yates, 1977; Emerich & Burris, 1978a, 1978b; Ludden, Okon, & Burris, 1978; Song, Hartman, & Burris, 1985). Thanks to advances in bioinformatics, researchers have conducted detailed sequence analyses of known nitrogenases and uncovered amino acid variances in mechanistically critical regions of the protein, including selenocysteine ligation to P-cluster and amino acid variability in the outer coordination sphere of FeMoco (Howard et al., 2013). We anticipate that the growing pool of genome sequences from diazotrophic bacteria will greatly augment the biochemical and structural investigation of the nitrogenase mechanism and possibly lead to the discovery of nitrogenases with novel chemistries.

ACKNOWLEDGMENTS

This work was supported by NIH (GM099813 to F.A.T.). F.A.T. also acknowledges the Frasch Foundation for further support. C.P.O. gratefully acknowledges support by USDA NIFA (Grant 2015-67012-22895). The authors also thank Michael Medina for his contributions and valuable discussions.

REFERENCES

Adams, P. D., Afonine, P. V., Bunkóczi, G., Chen, V. B., Davis, I. W., Echols, N., et al. (2010). PHENIX: A comprehensive Python-based system for macromolecular structure solution. *Acta Crystallographica. Section D, Biological Crystallography*, *66*, 213–221.

Battye, T. G., Kontogiannis, L., Johnson, O., Powell, H. R., & Leslie, A. G. (2011). iMOSFLM: A new graphical interface for diffraction-image processing with MOSFLM. *Acta Crystallographica. Section D, Biological Crystallography*, *67*, 271–281.

Bertalan, M., Albano, R., de Pádua, V., Rouws, L., Rojas, C., Hemerly, A., et al. (2009). Complete genome sequence of the sugarcane nitrogen-fixing endophyte *Gluconacetobacter diazotrophicus* Pal5. *BMC Genomics*, *10*, 450.

Bradford, M. M. (1976). A rapid and sensitive method for the quantitation of microgram quantities of protein utilizing the principle of protein-dye binding. *Analytical Biochemistry*, *72*, 248–254.

Brendt, H., Lowe, D. J., & Yates, M. G. (1977). The nitrogen-fixing system of *Corynebacterium autotrophicum*. *European Journal of Biochemistry*, *86*, 133–142.

Buren, S., Young, E. M., Sweeny, E. A., Lopez-Torrejon, G., Veldhuizen, M., Voigt, C. A., et al. (2017). Formation of nitrogenase NifDK tetramers in the mitochondria of Saccharomyces cerevisiae. *ACS Synthetic Biology*, *6*, 1043–1055.

Cavalcante, V. A., & Dobereiner, J. (1988). A new acid-tolerant nitrogen-fixing bacterium associated with sugarcane. *Plant and Soil*, *108*, 22–31.

Chan, J. M., Christiansen, J., Dean, D. R., & Seefeldt, L. C. (1999). Spectroscopic evidence for changes in the redox state of the nitrogenase P-cluster during turnover. *Biochemistry*, *38*, 5779–5785.

Chiu, H., Peters, J. W., Lanzilotta, W. N., Ryle, M. J., Seefeldt, L. C., Howard, J. B., et al. (2001). MgATP-bound and nucleotide-free structures of a nitrogenase protein complex between the Leu 127 Delta-Fe-protein and the MoFe-protein. *Biochemistry*, *40*, 641–650.

Danyal, K., Dean, D. R., Hoffman, B. M., & Seefeldt, L. C. (2011). Electron transfer within nitrogenase: Evidence for a deficit-spending mechanism. *Biochemistry*, *50*, 9255–9263.

Danyal, K., Mayweather, D., Dean, D. R., Seefeldt, L. C., & Hoffman, B. M. (2010). Conformational gating of electron transfer from the nitrogenase Fe protein to MoFe protein. *Journal of the American Chemical Society*, *132*, 6894–6895.

Danyal, K., Yang, Z. Y., & Seefeldt, L. C. (2011). Electron paramagnetic resonance spectroscopy. *Methods in Molecular Biology*, *766*, 191–205.

Dos Santos, P. C., Fang, Z., Mason, S. W., Setubal, J. C., & Dixon, R. (2012). Distribution of nitrogen fixation and nitrogenase-like sequences amongst microbial genomes. *BMC Genomics*, *13*, 162.

Duyvis, M. G., Wassink, H., & Haaker, H. (1996). Pre-steady-state kinetics of nitrogenase from *Azotobacter vinelandii*. Evidence for an ATP-induced conformational change of the nitrogenase complex as part of the reaction mechanism. *The Journal of Biological Chemistry*, *271*, 29,632–29,636.

Duyvis, M. G., Wassink, H., & Haaker, H. (1998). Nitrogenase of *Azotobacter vinelandii*: Kinetic analysis of the Fe protein redox cycle. *Biochemistry*, *37*, 17,345–17,354.

Einsle, O., Tezcan, F. A., Andrade, S. L., Schmid, B., Yoshida, M., Howard, J. B., et al. (2002). Nitrogenase MoFe-protein at 1.16 Å resolution: A central ligand in the FeMo-cofactor. *Science*, *297*, 1696–1700.

Emerich, D. W., & Burris, R. H. (1978a). Nitrogenase from Bacillus polymyxa. Purification and properties of the component proteins. *Biochimica et Biophysica Acta*, *536*, 172–183.

Emerich, D. W., & Burris, R. H. (1978b). Preparation of nitrogenase. *Methods in Enzymology*, *53*, 314–329.

Emsley, P., & Cowtan, K. (2004). Coot: Model-building tools for molecular graphics. *Acta Crystallographica. Section D, Biological Crystallography*, *60*, 2126–2132.

Emsley, P., Lohkamp, B., Scott, W. G., & Cowtan, K. (2010). Features and development of Coot. *Acta Crystallographica. Section D, Biological Crystallography*, *66*, 486–501.

Enemark, E. J., & Joshua-Tor, L. (2008). On helicases and other motor proteins. *Current Opinion in Structural Biology*, *18*, 243–257.

Evans, P. R., & Murshudov, G. N. (2013). How good are my data and what is the resolution? *Acta Crystallographica. Section D, Biological Crystallography*, *69*, 1204–1214.

Fisher, K., & Newton, W. E. (2005). Nitrogenase proteins from *Gluconacetobacter diazotrophicus*, a sugarcane-colonizing bacterium. *Biochimica et Biophysica Acta*, *1750*, 154–165.

Flores-Encarnacion, M., Contreras-Zentella, M., Soto-Urzua, L., Aguilar, G. R., Baca, B. E., & Escamilla, J. E. (1999). The respiratory system and diazotrophic activity of Acetobacter diazotrophicus PAL5. *Journal of Bacteriology*, *181*, 6987–6995.

Giongo, A., Tyler, H. L., Zipperer, U. N., & Triplett, E. W. (2010). Two genome sequences of the same bacterial strain, *Gluconacetobacter diazotrophicus* PAl 5, suggest a new standard in genome sequence submission. *Standards in Genomic Sciences*, *2*, 309–317.

Hall, S. R., Allen, F. H., & Brown, I. D. (1991). The crystallographic information file (CIF): A new standard archive file for crystallography. *Acta Crystallographica*, *A47*, 655–685.

Hamilton, T. L., Jacobson, M., Ludwig, M., Boyd, E. S., Bryant, D. A., Dean, D. R., et al. (2011). Differential accumulation of nif structural gene mRNA in *Azotobacter vinelandii*. *Journal of Bacteriology*, *193*, 4534–4536.

Hanson, P. I., & Whiteheart, S. W. (2005). AAA + proteins: Have engine, will work. *Nature Reviews. Molecular Cell Biology*, *6*, 519–529.

Hirsch, P. R., & Mauchline, T. H. (2015). The importance of the microbial N cycle in soil for crop plant nutrition. *Advances in Applied Microbiology*, *93*, 45–71.

Hoffman, B. M., Lukoyanov, D., Yang, Z.-Y., Dean, D. R., & Seefeldt, L. C. (2014). Mechanism of nitrogen fixation by nitrogenase: The next stage. *Chemical Reviews*, *114*, 4041–4062.

Howard, J. B., Kechris, K. J., Rees, D. C., & Glazer, A. N. (2013). Multiple amino acid sequence alignment nitrogenase component 1: Insights into phylogenetics and structure-function relationships. *PLoS One*, *8*, e72751.

Igarashi, R. Y., & Seefeldt, L. C. (2003). Nitrogen fixation: The mechanism of the Mo-dependent nitrogenase. *Critical Reviews in Biochemistry and Molecular Biology*, *38*, 351–384.

Kabsch, W. (2010). Integration, scaling, space-group assignment and post-refinement. *Acta Crystallographica. Section D, Biological Crystallography*, *66*, 133–144.

Katz, F. E. H., Owens, C. P., & Tezcan, F. A. (2016). Electron transfer reactions in biological nitrogen fixation. *Israel Journal of Chemistry*, *56*, 682–692.

Lanzilotta, W. N., Christiansen, J., Dean, D. R., & Seefeldt, L. C. (1998). Evidence for coupled electron and proton transfer in the [8Fe-7S] cluster of nitrogenase. *Biochemistry*, *37*, 11,376–11,384.

Lee, S., Reth, A., Meletzus, D., Sevilla, M., & Kennedy, C. (2000). Characterization of a major cluster of nif, fix, and associated genes in a sugarcane endophyte, Acetobacter diazotrophicus. *Journal of Bacteriology*, *182*, 7088–7091.

Lowe, D. J., & Thorneley, R. (1984). The mechanism of *Klebsiella pneumoniae* nitrogenase action. Pre-steady-state kinetics of H2 formation. *The Biochemical Journal*, *224*, 877–886.

Ludden, P. W., Okon, Y., & Burris, R. H. (1978). The nitrogenase system of *Spirillum lipoferum*. *The Biochemical Journal*, *173*, 1001–1003.

Mayer, S. M., Lawson, D. M., Gormal, C. A., Roe, S. M., & Smith, B. E. (1999). New insights into structure-function relationships in nitrogenase: A 1.6 Å resolution X-ray crystallographic study of *Klebsiella pneumoniae* MoFe-protein. *Journal of Molecular Biology*, *292*, 871–891.

Murshudov, G. N., Vagin, A. A., & Dodson, E. J. (1997). Refinement of macromolecular structures by the maximum-likelihood method. *Acta Crystallographica. Section D, Biological Crystallography*, *53*, 240–255.

Nicolet, Y., Rohac, R., Martin, L., & Fontecilla-Camps, J. C. (2013). X-ray snapshots of possible intermediates in the time course of synthesis and degradation of protein-bound Fe4S4 clusters. *Proceedings of the National Academy of Sciences of the United States of America*, *110*, 7188–7192.

Oldroyd, G. E. D., & Dixon, R. (2014). Biotechnological solutions to the nitrogen problem. *Current Opinion in Biotechnology*, *26*, 19–24.

Otwinowski, Z., & Minor, W. (1997). Processing of X-ray diffraction data collected in oscillation mode. *Methods in Enzymology*, *276*, 307–326.
Owens, C. P., Katz, F. E. H., Carter, C. H., Luca, M. A., & Tezcan, F. A. (2015). Evidence for functionally relevant encounter complexes in nitrogenase catalysis. *Journal of the American Chemical Society*, *137*, 12,704–12,712.
Owens, C. P., Katz, F. E., Carter, C. H., Oswald, V. F., & Tezcan, F. A. (2016). Tyrosine-coordinated P-cluster in G. diazotrophicus nitrogenase: Evidence for the importance of O-based ligands in conformationally gated electron transfer. *Journal of the American Chemical Society*, *138*, 10,124–7.
Pedraza, R. O. (2008). Recent advances in nitrogen-fixing acetic acid bacteria. *International Journal of Food Microbiology*, *125*, 25–35.
Peters, J. W., Stowell, M. H., Soltis, S. M., Finnegan, M. G., Johnson, M. K., & Rees, D. C. (1997). Redox-dependent structural changes in the nitrogenase P-cluster. *Biochemistry*, *36*, 1181–1187.
Rappas, M., Bose, D., & Zhang, X. (2007). Bacterial enhancer-binding proteins: Unlocking sigma54-dependent gene transcription. *Current Opinion in Structural Biology*, *17*, 110–116.
Raymond, J., Siefert, J. L., Staples, C. R., & Blankenship, R. E. (2004). The natural history of nitrogen fixation. *Molecular Biology and Evolution*, *21*, 541–554.
Rees, D. C., Akif Tezcan, F., Haynes, C. A., Walton, M. Y., Andrade, S., Einsle, O., et al. (2005). Structural basis of biological nitrogen fixation. *Philosophical Transactions of the Royal Society A: Mathematical, Physical and Engineering Sciences*, *363*, 971–984.
Reis, V. M., & Döbereiner, J. (1998). Effect of high sugar concentration on nitrogenase activity of Acetobacter diazotrophicus. *Archives of Microbiology*, *171*, 13–18.
Rogers, C., & Oldroyd, G. E. (2014). Synthetic biology approaches to engineering the nitrogen symbiosis in cereals. *Journal of Experimental Botany*, *65*, 1939–1946.
Roth, L. E., Nguyen, J. C., & Tezcan, F. A. (2010). ATP- and iron–protein-independent activation of nitrogenase catalysis by light. *Journal of the American Chemical Society*, *132*, 13,672–13,674.
Roth, L. E., & Tezcan, F. A. (2011). X-ray crystallography. *Methods in Molecular Biology (Clifton, N.J.)*, *766*, 147–164.
Roth, L. E., & Tezcan, F. A. (2012). ATP-uncoupled, six-electron photoreduction of hydrogen cyanide to methane by the molybdenum-iron protein. *Journal of the American Chemical Society*, *134*, 8416–8419.
Saravanan, V. S., Madhaiyan, M., Osborne, J., Thangaraju, M., & Sa, T. M. (2008). Ecological occurrence of *Gluconacetobacter diazotrophicus* and nitrogen-fixing Acetobacteraceae members: Their possible role in plant growth promotion. *Microbial Ecology*, *55*, 130–140.
Schindelin, H., Kisker, C., Schlessman, J. L., Howard, J. B., & Rees, D. C. (1997). Structure of ADP x AIF4(-)-stabilized nitrogenase complex and its implications for signal transduction. *Nature*, *387*, 370–376.
Seefeldt, L. C., Hoffman, B. M., & Dean, D. R. (2009). Mechanism of Mo-dependent nitrogenase. *Annual Review of Biochemistry*, *78*, 701–722.
Sevilla, M., Burris, R. H., Gunapala, N., & Kennedy, C. (2001). Comparison of benefit to sugarcane plant growth and 15N2 incorporation following inoculation of sterile plants with Acetobacter diazotrophicus wild-type and Nif- mutants strains. *Molecular Plant-Microbe Interactions: MPMI*, *14*, 358–366.
Song, S., Hartman, A., & Burris, R. H. (1985). Purification and properties of nitrogenase from *Azospirillum amazonense*. *Journal of Bacteriology*, *164*, 1271–1277.
Spatzal, T., Perez, K. A., Einsle, O., Howard, J. B., & Rees, D. C. (2014). Ligand binding to the FeMo-cofactor: Structures of CO-bound and reactivated nitrogenase. *Science*, *345*, 1620–1623.

Tejera, N. A., Ortega, E., Rodes, R., & Lluch, C. (2004). Influence of carbon and nitrogen sources on growth, nitrogenase activity, and carbon metabolism of *Gluconacetobacter diazotrophicus*. *Canadian Journal of Microbiology*, *50*, 745–750.

Tezcan, F. A., Kaiser, J. T., Howard, J. B., & Rees, D. C. (2015). Structural evidence for asymmetrical nucleotide interactions in nitrogenase. *Journal of the American Chemical Society*, *137*, 146–149.

Tezcan, F. A., Kaiser, J. T., Mustafi, D., Walton, M. Y., Howard, J. B., & Rees, D. C. (2005). Nitrogenase complexes: Multiple docking sites for a nucleotide switch protein. *Science (New York, N.Y.)*, *309*, 1377–1380.

Thorneley, R. N., & Lowe, D. J. (1983). Nitrogenase of *Klebsiella pneumoniae*. Kinetics of the dissociation of oxidized iron protein from molybdenum-iron protein: Identification of the rate-limiting step for substrate reduction. *Biochemical Journal*, *215*, 393–403.

Ubbink, M. (2009). The courtship of proteins: Understanding the encounter complex. *FEBS Letters*, *583*, 1060–1066.

Wang, L., Zhang, L., Liu, Z., Zhao, D., Liu, X., Zhang, B., et al. (2013). A minimal nitrogen fixation gene cluster from Paenibacillus sp. WLY78 enables expression of active nitrogenase in Escherichia coli. *PLoS Genetics*, *9*, e1003865.

Willing, A. H., Georgiadis, M. M., Rees, D. C., & Howard, J. B. (1989). Cross-linking of nitrogenase components. Structure and activity of the covalent complex. *The Journal of Biological Chemistry*, *264*, 8499–8503.

Willing, A., & Howard, J. B. (1990). Cross-linking site in *Azotobacter vinelandii* complex. *The Journal of Biological Chemistry*, *265*, 6596–6599.

Wilson, P. E., Nyborg, A. C., & Watt, G. D. (2001). Duplication and extension of the Thorneley and Lowe kinetic model for *Klebsiella pneumoniae* nitrogenase catalysis using a mathematica software platform. *Biophysical Chemistry*, *91*, 281–304.

Winn, M. D., Ballard, C. C., Cowtan, K. D., Dodson, E. J., Emsley, P., Evans, P. R., et al. (2011). Overview of the CCP4 suite and current developments. *Acta Crystallographica. Section D, Biological Crystallography*, *67*, 235–242.

Zhang, L. M., Morrison, C. N., Kaiser, J. T., & Rees, D. C. (2015). Nitrogenase MoFe protein from *Clostridium pasteurianum* at 1.08 A resolution: Comparison with the *Azotobacter vinelandii* MoFe protein. *Acta Crystallographica. Section D, Biological Crystallography*, *71*, 274–282.